Electronic Supplementary Material (ESI) for Inorganic Chemistry Frontiers.

Supplementary data

Water-mediated reduction of $[Cu(dmp)_2(CH_3CN)]^{2+}$: Implications of the structure of a classical complex on its activity as an anticancer drug

Pedro Levín,[†[a]] María C. Ruiz,[†[b]] Adolfo I. B. Romo,[[c]] Otaciro R. Nascimento,[[d]] Ana L. Di Virgilio,[[b]] Allen G. Oliver,[[e]] Alejandro P. Ayala,[[f]] Izaura C. N. Diogenes,[*[c]] Ignacio E. León,[*[b]] Luis Lemus[*[a]]

[a] Departamento química de los materiales, Facultad de Química y Biología, Universidad de Santiago de Chile, Av. Libertador Bernardo O'Higgins 3363, Estación Central, Santiago, Chile.
E-mail: luis.lemus@usach.cl

[b] Centro de Química Inorgánica CEQUINOR (CONICET-UNLP), Bv 120 1465 1900, La Plata, Argentina.
E-mail: e-mail: ileon@biol.unlp.edu.ar

[c] Departamento de Química Orgânica e Inorgânica Universidade Federal do Ceará, Cx. Postal 6021 Fortaleza, CE, 60451-970, Brazil.
E-mail: izaura@dqoi.ufc.br

[d] Departamento de Física Interdiciplinar, Instituto de Física de São Carlos Universidade de São Paulo, CP 369, CEP 13560-970 São Carlos, SP, Brazil.

[e] Department of Chemistry and Biochemistry, University of Notre Dame, 46556-5670 Notre Dame, IN, USA.

[f] Departamento de Física Universidade Federal do Ceará, Fortaleza, CE, 65455-900, Brazil.

† Coauthors contributed equally to this work.

* Corresponding Authors:

Luis Lemus, e-mail: luis.lemus@usach.cl

Ignacio E. León, e-mail: ileon@biol.unlp.edu.ar

Izaura C. N. Diogenes, e-mail: izaura@dqoi.ufc.br

Crystallographic structures

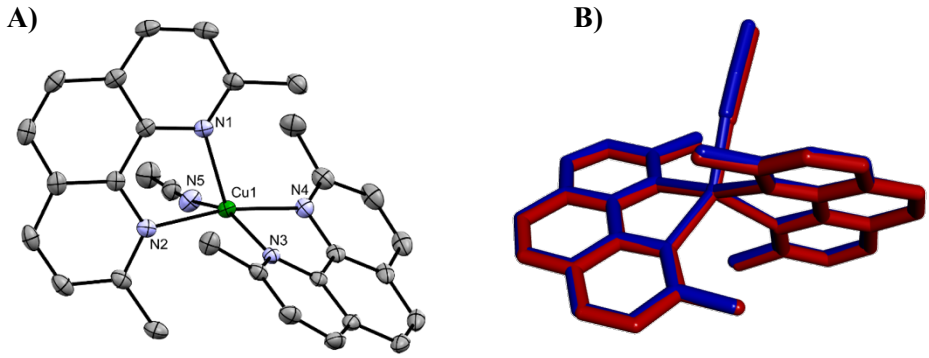

Figure S1. A) ORTEP diagram of the molecular structure of $[Cu(dmp)(CH_3CN)](ClO_4)_2$ reported in this work. B) Overlay of the structure of this work (red) with the previously reported (blue).[1]

EPR and UV-vis measurements

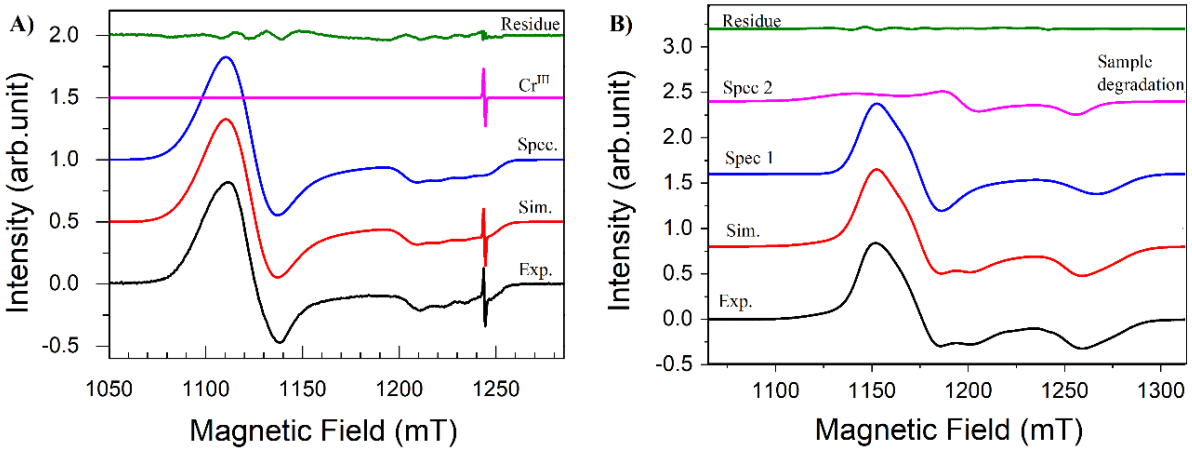

Figure S2. EPR spectra in solid state of A) $[Cu(dmp)_2(CH_3CN)](ClO_4)_2$ and B) $[Cu(phen)_2(CH_3CN)](ClO_4)_2$. Experimental in black line, simulated spectra in red line and principal species in blue line. Spectral simulations were made with the EasySpin program.[2] The pink line in the A figure corresponds to MgO:Cr^{III} used as g marker (g=1.9797) to calibrate the magnetic field.

EPR spectra of $[Cu(phen)_2(ClO_4)](ClO_4)_2$ and $[Cu(dmp)_2(ClO_4)](ClO_4)_2$ in the solid state were recorded at 298 K in a Varian E-110 Q-band instrument with a cylindrical cavity, and a frequency of 35.48950 and 34.47017 GHz, respectively. The sample (around 2 mg) was transferred to a quartz capillary tube (1 mm internal diameter) before being inserted into the spectrometer cavity; microwave power 10 mW; modulation amplitude 0.4 mT. Spectral simulations were made by using the EasySpin program.[2] The R parameter value was determined by using $(g_y-g_z)/(g_x-g_y)$.[3,4]

Both complexes show rhombic spectra, in agreement with a pentacoordinated Cu^{II} center in a geometry intermediate between TBPY-5 and SPY-5. For $[Cu(dmp)_2(CH_3CN)](ClO_4)_2$, calculated *g* tensor values are g_x=2.223, g_y=2.193, g_z=2.008 and R=6.17. For $[Cu(phen)_2(CH_3CN)](ClO_4)_2$ *g* values are g_x=2.203, g_y=2.156, g_z=2.000, and R=3.32. The ground state in both compounds is composed by a linear combination of the d_{z^2} and $d_{x^2-y^2}$ orbitals, however, the R parameters are indicative that the main contribution arises from the d_{z^2} orbital as the ground state,[3] which is related to geometries closer to the TBPY-5.

In $[Cu(phen)_2(CH_3CN)](ClO_4)_2$ the geometry is closer to a TBPY-5 with each phenanthroline ligand providing an equatorial and an axial nitrogen around Cu^{II}. The fifth coordination site is occupied by a CH_3CN fragment. The calculated g_z value of is close to the free electron ($g_e = g_{free\ electron} = 2.0023$), which also indicates that the unpaired electron is in d_z^2, due to the crystal field generated by the ligands in a TBPY-5 geometry. It was also possible to observe in the EPR spectrum, a small amount of sample corresponding to secondary species of Cu^{II} (g_x=2.228, g_y=2.121, g_z=2.018, R = 0.95) (fig. S2 B, pink line). Probably, the molecule undergoes an exchange of the fifth ligand for a molecule of water, which increases the contribution of the d_x^2-$_y^2$ orbital.[3,5,6,7] On the other hand, the solid was presumably not sufficiently magnetically diluted to yield EPR spectra indicative of the weak exchange between neighbor molecules, producing collapse of Cu nuclear (I = 3/2) hyperfine lines.

For $[Cu(dmp)_2(CH_3CN)](ClO_4)$, the main contribution to the ground-state HOMO arises from the d_z^2, acccording to the R values calculated. However, this complex presents a slightly higher degree of distortion from the TBPY-5 geometry, mainly due to the steric hindrance imparted by the methyl groups in the dmp ligand. Furthermore, it was possible to obtain hyperfine couplings for this complex, presenting values A_x = 20.6 G, A_y = 21.0 G and A_z = 123.5 G. The A parameters are typical of a Cu^{II} complex in a predominantly axially elongated five-coordinate geometry ($g_z \sim g_e < (g_x, g_y)$, $A_z \gg A_y \sim A_x$) and consistent with a d_z^2 electronic ground state. Hyperfine coupling with the Cu nucleus (I = 3/2) is resolved in the z-direction and the large A_z value (123.5 G) rules a trigonal bipyramidal coordination geometry.[5,6]

The EPR spectra recorded in acetonitrile/H_2O mixtures at 77 K (fig. S3), show magnetic interaction between molecules of complex. For $[Cu(dmp)_2(CH_3CN)](ClO_4)_2$ g values calculated are g_x=2.106, g_y=2.134, g_z=2.162, and R=1.00. For $[Cu(phen)_2(CH_3CN)](ClO_4)_2$ *g* values are g_x=2.064, g_y=2.123, g_z=2.189, and R=1.12. In both complexes, a change in the geometry and inversion of the *g* tensor values was observed ($g_x < g_y < g_z$). probably due to the exchange of coordinated acetonitrile by water. The *g* parameters are typical for a Cu(II) complexes in a predominantly axially elongated five-coordinate geometry with additional rhombic distortion ($g_z > g_y > g_x$,) and consistent with a $d_x^2-_y^2$ electronic ground state.[6,8]

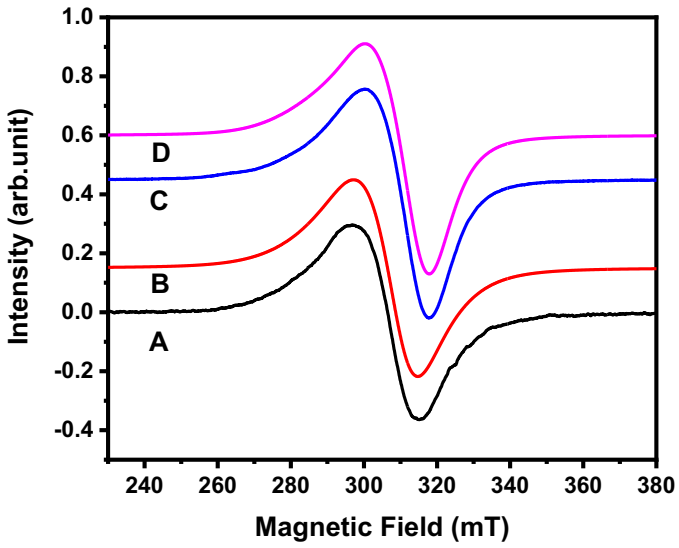

Figure S3. EPR spectra in acetonitrile/H_2O solution at 77 K (liquid nitrogen) of $[Cu(dmp)_2(CH_3CN)](ClO_4)_2$ **A)** and $[Cu(phen)_2(CH_3CN)](ClO_4)_2$ **C)**. Spectral simulations **B** and **D**, were made with the EasySpin program[2] with the following EPR parameters: Freq.= 9.11009 GHz, g = [2.106 2.134 2.162], Lw = [37.4 73.3] Gauss and Freq.= 9.11063 GHz, g = [2.064 2.123 2.189], Lw = [49.9 49.2] Gauss , respectively.

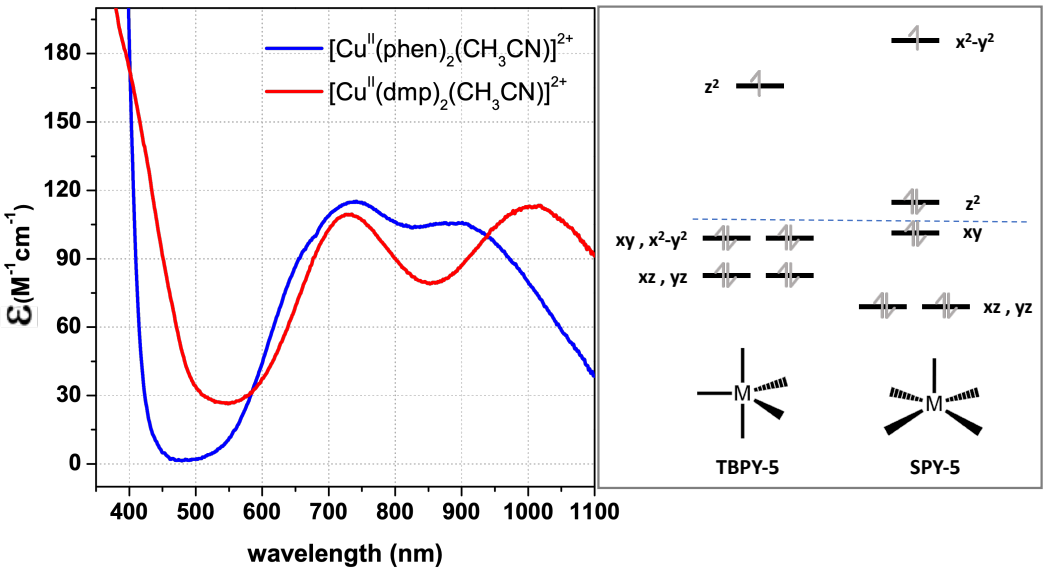

Figure S4. Left: Electronic spectra of $[Cu(dmp)_2(CH_3CN)]^{2+}$ (red) and $[Cu(phen)_2(CH_3CN)]^{2+}$ (blue), in the range of wavelengths where d-d transitions are observed. In the red spectrum, absorptions in the range 400-500 nm are due to the presence of a small amount of $[Cu(dmp)_2]^{+}$ produced by spontaneous reduction of the cupric complex. Right: Splitting of *d* orbitals for a pentacordinated Cu^{II} ion (d^9) in limit geometries of TBPY-5 and SPY-5, based on ligand field theory.

Crystallographic information for $[Cu(phen)_2(CH_3CN)](ClO_4)_2$ and $[Cu(dmp)_2](ClO_4)$ · toluene.

Table S1. Comparison of selected bonds distances (Å) and angles (deg).

$[Cu(phen)_2(CH_3CN)]^{2+}$	Bonds	$[Cu(dmp)_2]^{+}$	Bonds
Cu1-N1	1.9808(12)	Cu(1)-N(1)#1	2.021(2)
Cu1-N2	2.0848(12)	Cu(1)-N(2)#1	2.040(3)
Cu1-N1#	1.9808(12)	Cu(1)-N(1)	2.021(2)
Cu1-N2#	2.0848(12)	Cu(1)-N(2)	2.040(3)
Cu1-N3 (CH_3CN)	2.0644(18)		
$[Cu(phen)_2(CH_3CN)]^{2+}$	Angles	$[Cu(dmp)_2]^{+}$	Angles
N2-Cu1-N2#	117.20 (6)	N(1)#1-Cu(1)-N(1)	127.41(12)
N3-Cu1-N2#	121.40 (3)	N(1)#1-Cu(1)-N(2)#1	82.96(11)
N3-Cu1-N2	121.40 (3)	N(1)-Cu(1)-N(2)#1	120.40(10)
N1-Cu1-N2	81.67 (5)	N(1)#1-Cu(1)-N(2)	120.40(10)
N1-Cu1-N2#	96.52 (5)	N(1)-Cu(1)-N(2)	82.96(11)
N1#-Cu1-N2#	81.67 (5)	N(2)#1-Cu(1)-N(2)	128.70(14)
N1#-Cu1-N2	96.52 (5)		
N1#-Cu1-N3	91.73 (3)		
N1-Cu1-N3	91.73 (3)		
N1-Cu1-N1#	176.55 (6)		

Table S2. Crystallographic information.

Compound	$[Cu(\mathbf{phen})_2(CH_3CN)](ClO_4)_2$	$[Cu(\mathbf{dmp})_2](ClO_4)\cdot$ toluene
Empirical formula	$C_{26}H_{19}Cl_2CuN_5O_8$	$C_{35}H_{32}ClCuN_4O_4$
Formula weight	663.90 g/mol	671.63
Temperature		102(2) K
Wavelength	0.71073 Å	0.71073 Å
Crystal system	Monoclinic	Monoclinic
Space group	C2/c	C2/c
Unit cell dimensions	*a* = 19.7424(10) Å, α = 90°	*a* = 16.062(2) Å α = 90°
	b = 8.6861(5) Å, β = 98.024(2)°	*b* = 15.334(2) Åβ = 106.724(2)°
	c = 15.1100(8) Å, γ = 90°	*c* = 13.3409(19) Å, γ = 90°
Volume	2565.8(2) $Å^3$	3146.9(8) $Å^3$
Z	4	4
Density (calculated)	1.719 g/cm^3	1.418 $g.cm^{-3}$
Absorption coefficient (μ)	1.123 mm^{-1}	0.825 mm^{-1}
F(000)	1348	1392
Crystal size	0.228 x 0.323 x 0.403 mm^3	0.22 × 0.17 × 0.13 mm^3
θ range for data collection	2.84 to 30.66°	1.88 to 26.84°
Index ranges	-24 ≤h ≤ 28, -12 ≤ k≤ 12, -21 ≤ l ≤21	-20 ≤ h ≤ 17, -19 ≤ k ≤ 19, -16 ≤ l ≤ 16
Reflections collected	22906	11338
Independent reflections	3952 [R_{int} = 0.0343]	3346 [R_{int} = 0.0214]
Completeness to θ = 27.00°	99.4%	99.1 %
Absorption correction	Numerical	Empirical
Max. and min. transmission	0.7169 and 0.5691	0.9004 and 0.8394
Refinement method	Full-matrix least-squares on F^2	Full-matrix least-squares on F^2
Data / restraints / parameters	3952 / 0 / 230	3346 / 0 / 226
Goodness-of-fit on F^2	1057	1048
Final R indices [I>2σ(I)]	R_1 = 0.0326, wR_2 = 0.0952	R_1 = 0.0471, wR_2 = 0.1300
R indices (all data)	R_1 = 0.0374, wR_2 = 0.0999	R_1 = 0.0635, wR_2 = 0.1437
Largest diff. peak and hole	0.360 and -0.771 $e^-Å^{-3}$	0.707 and -0.404 $e^-.Å^{-3}$

Spectral changes in acetonitrile solutions of $[Cu(dmp)_2(CH_3CN)]^{2+}$ containing variable amounts of water.

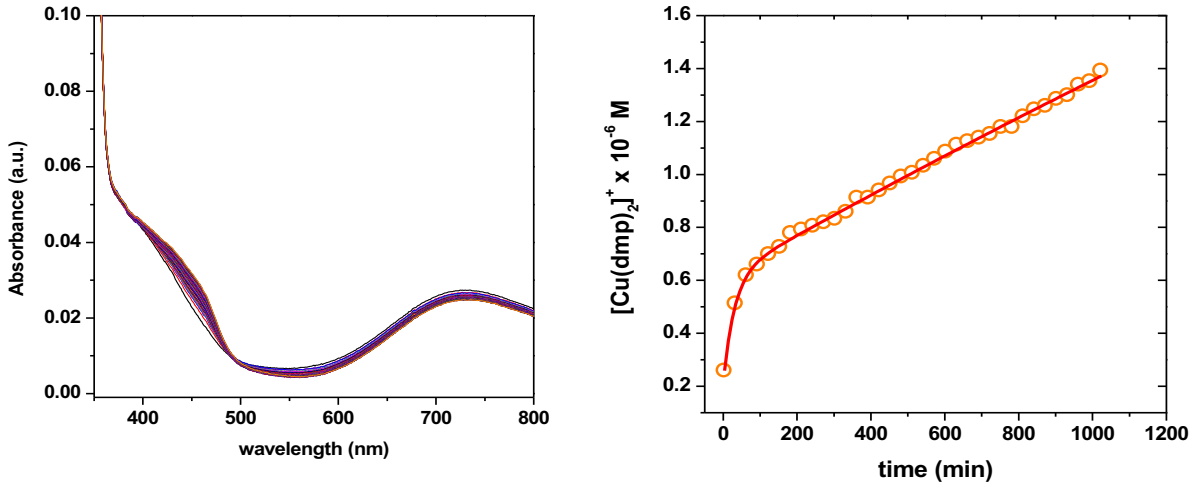

Figure S5. Spectral variation of $[Cu(dmp)_2(CH_3CN)]^{2+}$ 2.5x10^{-4} M in acetonitrile (no added water). Kinetic profile of formation of $[Cu(dmp)_2]^+$ and biexponential decay fit. Calculated τ_1 = 30.09 min^{-1}, τ_2 = 7687.5 min^{-1}.

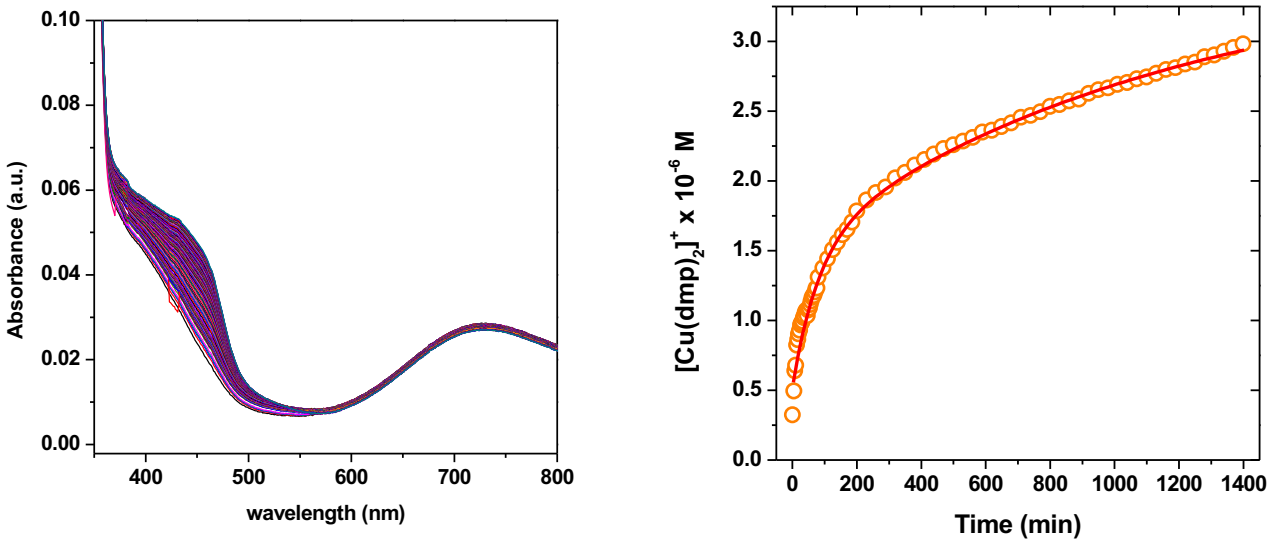

Figure S6. Spectral variation of $[Cu(dmp)_2(CH_3CN)]^{2+}$ 2.5x10^{-4} M in acetonitrile + 10 equiv H_2O. Kinetic profile of formation of $[Cu(dmp)_2]^+$ and biexponential decay fit. Calculated τ_1 = 79.57 min^{-1}, τ_2 = 1150.2 min^{-1}.

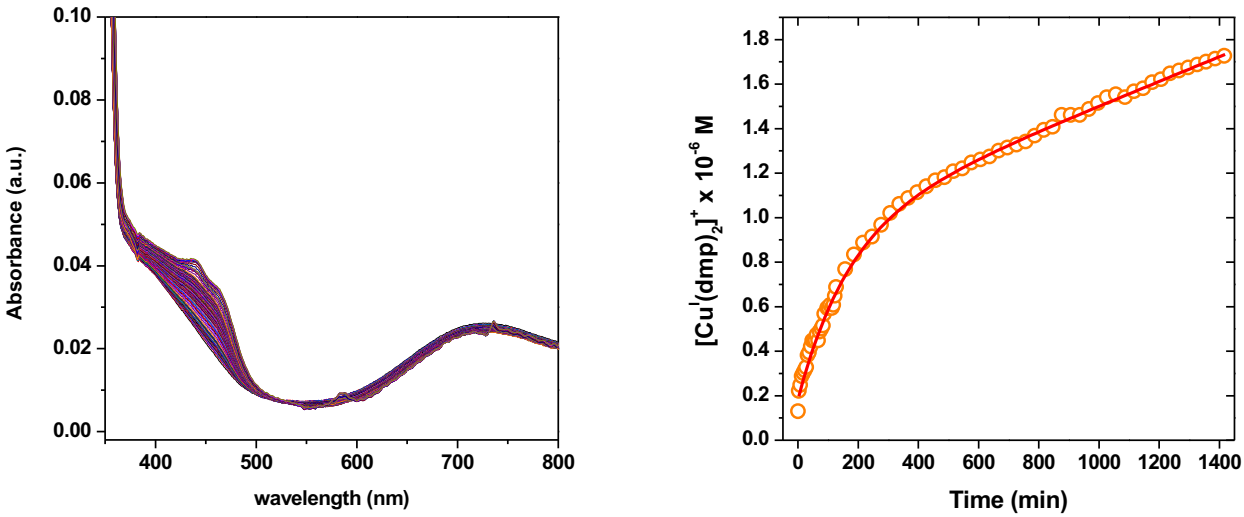

Figure S7. Spectral variation of $[Cu(dmp)_2(CH_3CN)]^{2+}$ 2.5x10^{-4} M in acetonitrile + 30 equiv H_2O. Kinetic profile of formation of $[Cu(dmp)_2]^+$ and biexponential decay fit. Calculated τ_1 = 165.38 min^{-1}, τ_2 = 3.00x10^7 min^{-1}.

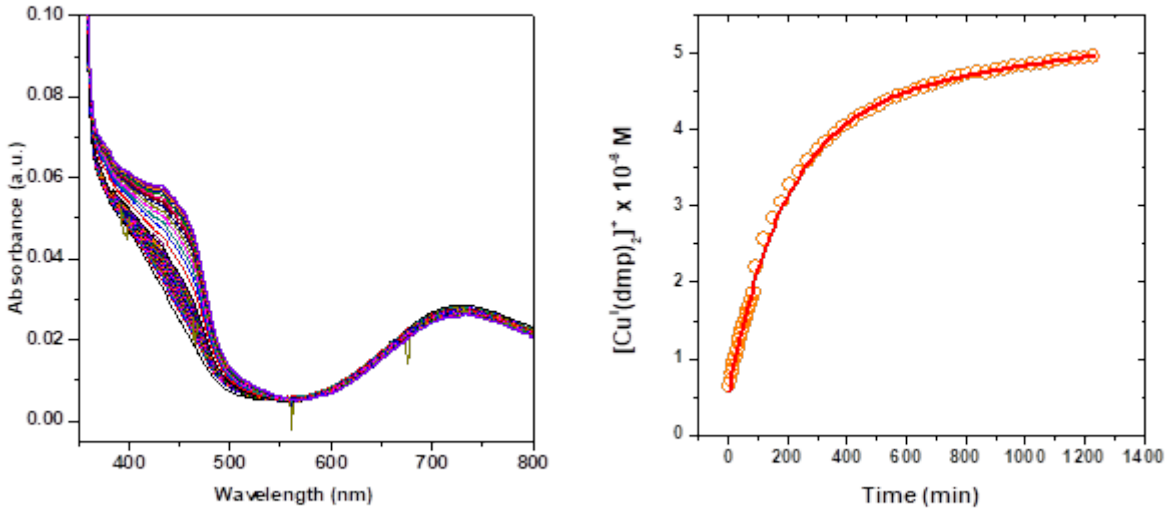

Figure S8. Spectral variation of $[Cu(dmp)_2(CH_3CN)]^{2+}$ 2.5x10^{-4} M in acetonitrile + 50 equiv H_2O. Kinetic profile of formation of $[Cu(dmp)_2]^+$ and biexponential decay fit. Calculated τ_1 = 189.8 min^{-1}, τ_2 = 3.18 x10^4 min^{-1}.

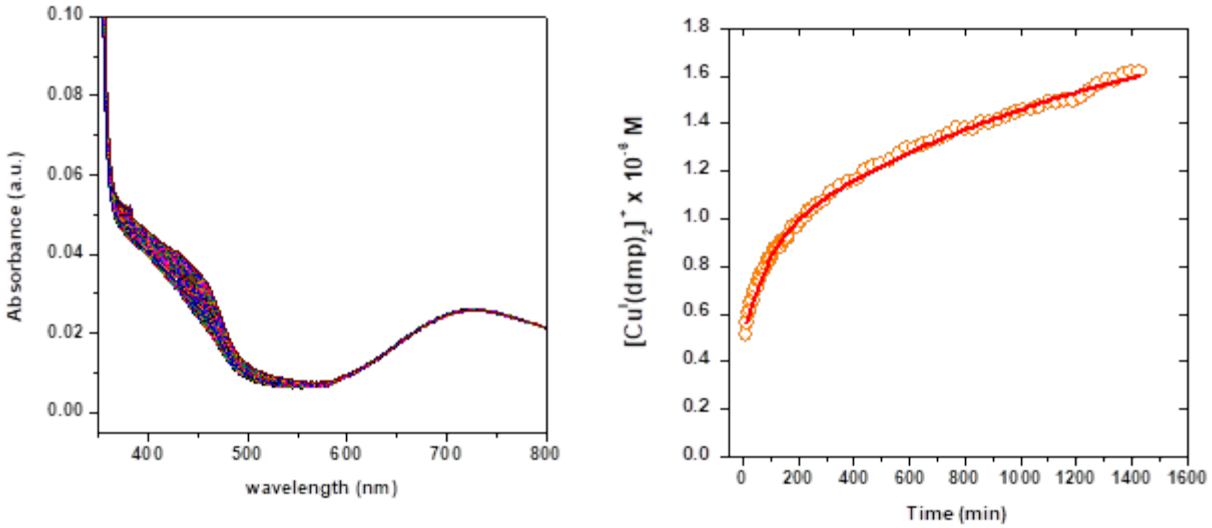

Figure S9. Spectral variation of $[Cu(dmp)_2(CH_3CN)]^{2+}$ 2.5x10^{-4} M in acetonitrile + 80 equiv H_2O. Kinetic profile of formation of $[Cu(dmp)_2]^+$ and biexponential decay fit. Calculated τ_1 = 98.38 min^{-1}, τ_2 = 1333 min^{-1}.

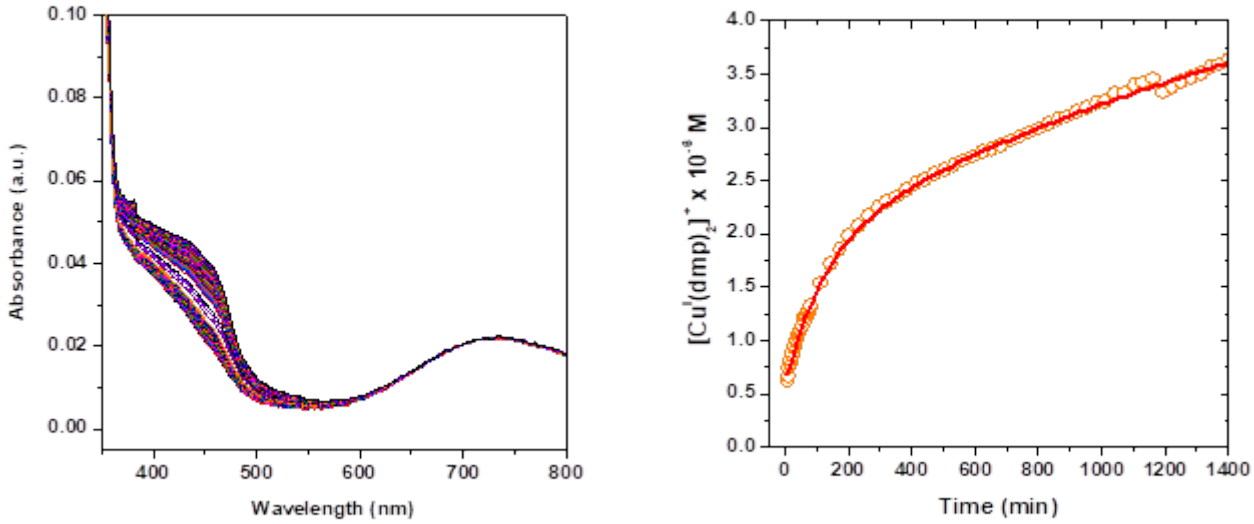

Figure S10. Spectral variation of $[Cu(dmp)_2(CH_3CN)]^{2+}$ 2.5x10^{-4} M in acetonitrile + 100 equiv H_2O. Kinetic profile of formation of $[Cu(dmp)_2]^+$ and biexponential decay fit. Calculated τ_1 = 121 min^{-1}, τ_2 = 2163.7 min^{-1}.

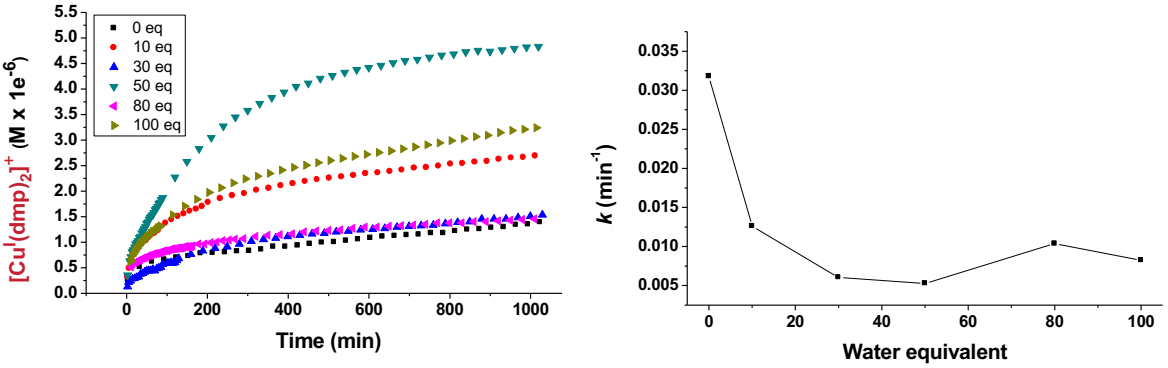

Figure S11. Left: Kinetic profile of formation of $[Cu(dmp)_2]^+$ at different amount of water, followed at A_{obs}=456 nm. Right: Rate constants of formation of $[Cu(dmp)_2]^+$as a function of the equivalents of water.

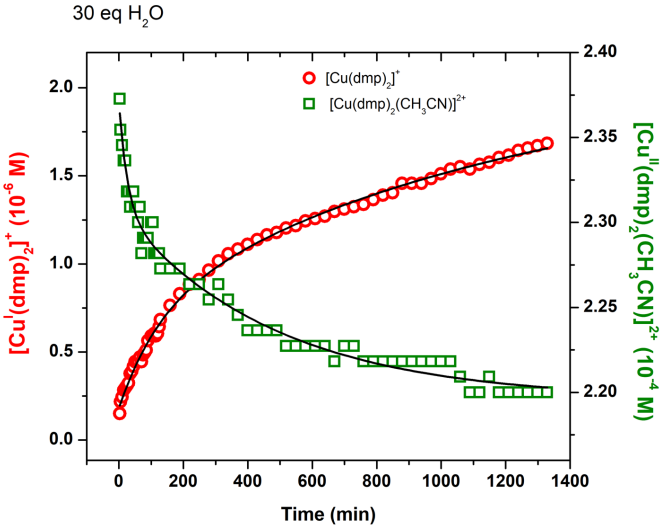

Figure S12. Kinetic profiles for the formation of $[Cu(dmp)_2]^+$ (red circles, λ_{obs}=456 nm), and consumption of $[Cu(dmp)_2(CH_3CN)]^{2+}$ (green squares, λ_{obs}=727 nm), in an acetonitrile solution $2.5x10^{-4}$ M of $[Cu(dmp)_2(CH_3CN)]^{2+}$ after addition of 30 eq of water. A biexponential equation was used to fit both profiles (black curves).

Table S3. Observed rate constants calculated by biexponential fit of the formation of $[Cu(dmp)_2]^+$ and decay of $[Cu(dmp)_2(CH_3CN)]^{2+}$ (figure 1). Variation in the concentration of each species was calculated at 1200 min of reaction, being (+) formation and (-) decrease from the initial concentration of complex.

+ 30 eq H_2O	$k_{obs\ 1}$	$k_{obs\ 2}$	Variation in the complex concentration after 1200 min
$[Cu(dmp)_2]^+$	$8.1x10^{-3}$	$8.7x10^{-4}$	(+) $1.6x10^{-6}$ M
$[Cu(dmp)_2(CH_3CN)]^{2+}$	$3.9x10^{-2}$	$2.1x10^{-3}$	(-) $1.7x10^{-5}$ M

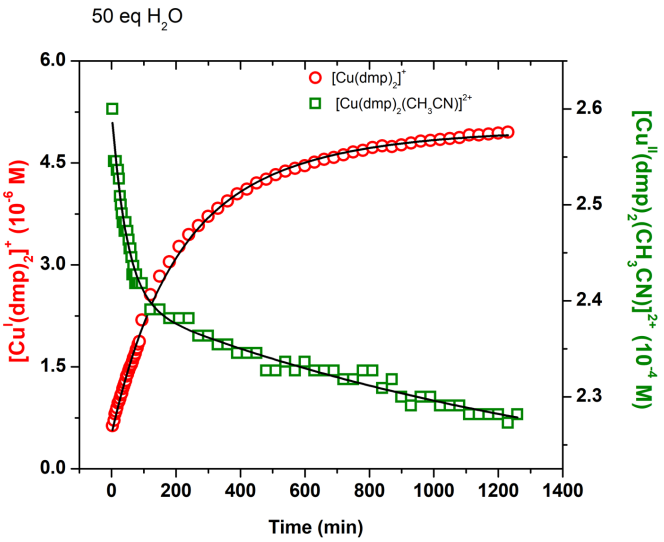

Figure S13. Kinetic profiles for the formation of $[Cu(dmp)_2]^+$ (red circles, λ_{obs}=456 nm), and consumption of $[Cu(dmp)_2(CH_3CN)]^{2+}$ (green squares, λ_{obs}=727 nm), in an acetonitrile solution $2.5x10^{-4}$ M of $[Cu(dmp)_2(CH_3CN)]^{2+}$ after addition of 50 eq of water. A biexponential equation was used to fit both profiles (black curves).

Table S4. Observed rate constants calculated by biexponential fit of the formation of $[Cu(dmp)_2]^+$ and decay of $[Cu(dmp)_2(CH_3CN)]^{2+}$ (figure 1). Variation in the concentration of each species was calculated at 1200 min of reaction, being (+) formation and (-) decrease from the initial concentration of complex.

+ 50 eq H_2O	$k_{obs\ 1}$	$k_{obs\ 2}$	Variation in the complex concentration after 1200 min
$[Cu(dmp)_2]^+$	$6.8x10^{-3}$	$2.7x10^{-3}$	(+) $4.9x10^{-6}$ M
$[Cu(dmp)_2(CH_3CN)]^{2+}$	$2.2x10^{-2}$	$6.6x10^{-4}$	(-) $3.2x10^{-5}$ M

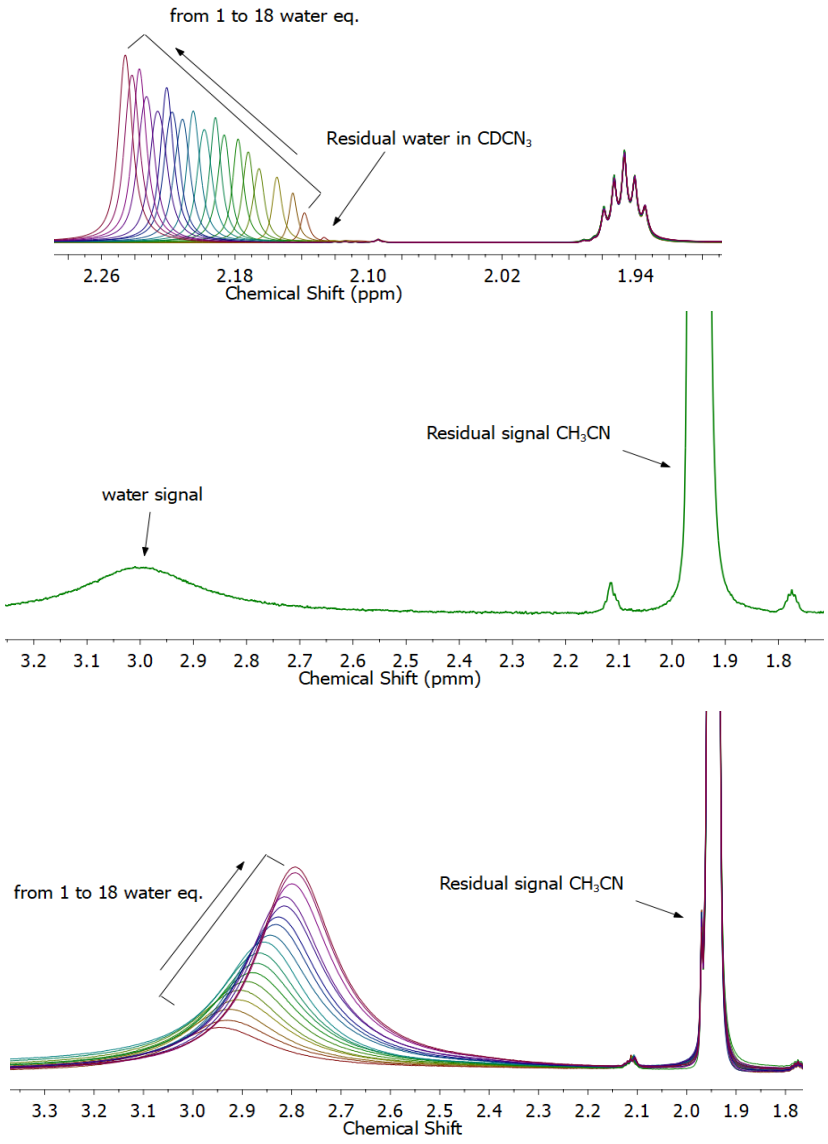

Figure S14. Above: ^{1}H-NMR spectra of CD_3CN with additions of water (without complex). Center: ^{1}H-NMR spectra of an CD_3CN solution of $[Cu(dmp)_2(CH_3CN)](ClO_4)_2$. Below: ^{1}H-NMR spectra of an CD_3CN solution of $[Cu(dmp)_2(CH_3CN)](ClO_4)_2$ with additions of equivalent amounts of water.

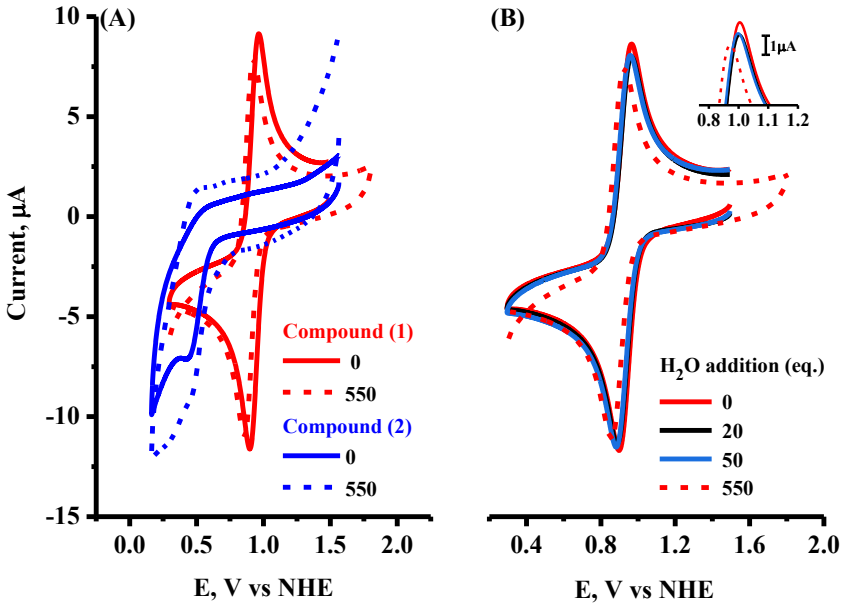

Figure S15. Cyclic voltammograms (CVs) at 100 mV s^{-1} in acetonitrile containing 0.1 mol L^{-1} TBAP and 0.001 mol L^{-1} solutions of $[Cu(dmp)_2(CH_3CN)]^{2+}$ (compound 1) and $[Cu(phen)_2(CH_3CN)]^{2+}$ (compound 2). Panel (A): CVs obtained before (solid lines) and after (dashed lines) addition of 550 equivalents of water. Panel (B): CVs during water addition in the solution containing $[Cu(dmp)_2(CH_3CN)]^{2+}$ after addition of different amount of water, as indicated. Inset: zoom in to show the potential shifts of the oxidative peaks during water addition.

Table S5. Shape measurements for the Cu-N_4 core in $[Cu(dmp)_2(CH_3CN)]^{2+}$ and $[Cu(phen)_2(CH_3CN)]^{2+}$ with no coordinated CH_3CN, and $[Cu(dmp)_2]^+$.

Compound (CCDC deposition number)	SP-4	vTBPY-4	T-4	SS-4	Reference
$[Cu(dmp)_2(CH_3CN)]^{2+}$	16.755	8.239	9.408	2.784	**this work**
$[Cu(dmp)_2(CH_3CN)]^{2+}$	16.699	8.390	9.239	2.654	1
$[Cu(phen)_2(CH_3CN)]^{2+}$	9.277	14.124	13.838	3.212	**this work**
$[Cu(dmp)_2]^+$	22.356	8.632	5.474	8.278	**this work**
$[Cu(dmp)_2]^+$ (278537)	21.923	8.254	5.787	8.494	9
$[Cu(dmp)_2]^+$ (278538)	25.156	8.451	5.487	9.511	9
$[Cu(dmp)_2]^+$ (228941)	25.227	7.347	5.343	8.493	10
$[Cu(dmp)_2]^+$ (228942)	21.962	7.580	6.176	7.019	10
$[Cu(dmp)_2]^+$ (228943)	23.022	8.041	5.779	8.033	10
$[Cu(dmp)_2]^+$ (228944)	21.119	8.215	6.201	7.960	10
$[Cu(dmp)_2]^+$ (228945)	20.344	7.855	6.650	7.587	10
$[Cu(dmp)_2]^+$ (228947)	20.436	8.172	6.041	7.422	10
$[Cu(dmp)_2]^+$ (228948)	24.907	8.041	5.300	8.838	10
$[Cu(dmp)_2]^+$ (228949)	24.609	8.050	5.420	9.113	10
$[Cu(dmp)_2]^+$ (228950a)	21.935	8.010	6.124	7.361	10
$[Cu(dmp)_2]^+$ (228950b)	25.875	7.429	5.824	7.108	10
$[Cu(dmp)_2]^+$ (228951)	17.856	9.141	6.527	7.075	10

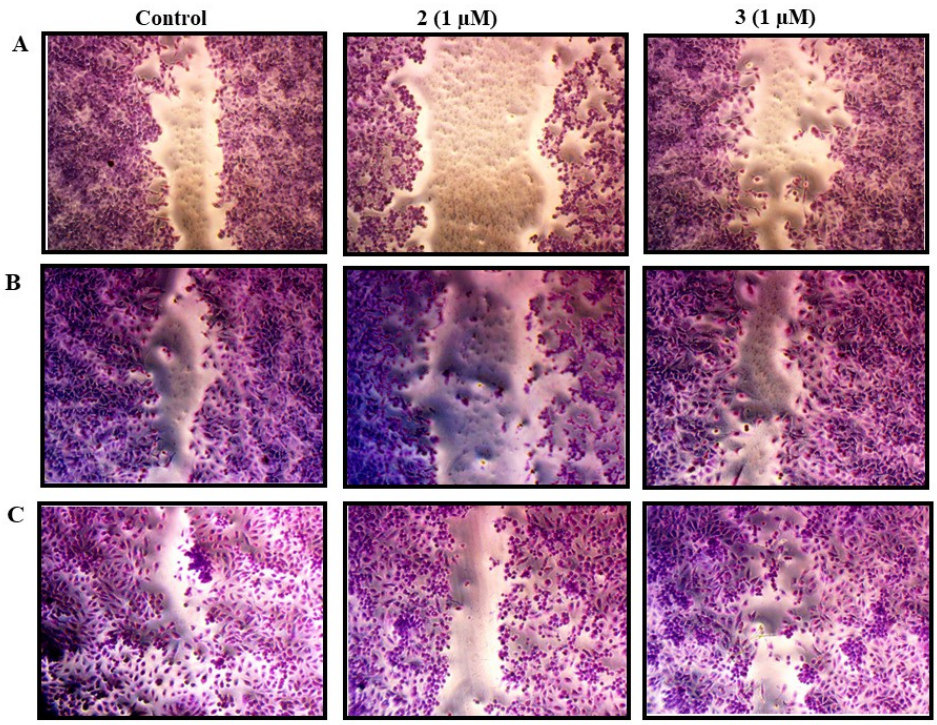

Figure S16. Wound healing assay. (A) MG-63, (B) A549 and (C) MDA-MB-231.

References

1 V. Leandri, Q. Daniel, H. Chen, L. Sun, J. M. Gardner and L. Kloo, *Inorg. Chem.* 2018, 57, 4556–4562.

2 S. Stoll and A. Schweiger, *J. Magn. Reson.* 2006, 178, 42–55.

3 E. Garribba and G. Micera, *J. Chem. Educ.* 2006, 83, 1229–1232.

4 B. J. Hathaway and A. G. Tomlinson, *Coord. Chem. Rev.* 1970, 5, 1–43.

5 Y. Yao, M. W. Perkovic, D. P. Rillema and C. Woods, *Inorg. Chem.* 1992, 31, 3956–3962.

6 M. Pitié, C. Boldron, H. Gornitzka, C. Hemmert, B. Donnadieu and B. Meunier, *Eur. J. Inorg. Chem.* 2003, 528–540.

7 A. I. B. Romo, D. S. Abreu, T. de F. Paulo, M. S. P. Carepo, E. H. S. Sousa, L. Lemus, C. Aliaga, A. A. Batista, O. R. Nascimento, H. D. Abruña and I. C. N. Diógenes, *Chem. - A Eur. J.* 2016, 22, 10081–10089.

8 A. I. B. Romo, V. S. Dibo, D. S. Abreu, M. S. P. Carepo, A. C. Neira, I. Castillo, L. Lemus, O. R. Nascimiento, P. V. Bernhardt, E. H. S. Sousa and I. C. N. Diógenes, *Dalton Trans.* 2019, 48, 14128–14137.

9 G. King, M. Gembicky and P. Coppens, *Acta Crystallogr. Sect. C Cryst. Struct. Commun.* 2005, 61, 329–332.

10 A. Y. Kovalevsky, M. Gembicky, I. V. Novozhilova and P. Coppens, *Inorg. Chem.* 2003, 42, 8794–8802.